Observation of the charged defect migration that causes the degradation of double-Schottky barriers using a nondestructive quantitative profiling technique

Chenlu Cheng, Jinliang He,[a] and Jun Hu
State Key Laboratory of Power System, Department of Electrical Engineering, Tsinghua University, Beijing 100084, China

(Received 21 July 2014; accepted 22 September 2014; published online 30 September 2014)

The migration and neutralization of charged defect ions during the degradation of a double-Schottky barrier are observed by performing nondestructive pulsed electroacoustic measurements on ZnO bicrystals. This offers the possibility to experimentally access the predicted defect migration behavior and provides a solid foundation to validate the theoretical aging model for electroceramics. Theoretical modeling of the acoustic attenuation effects during measurements is also discussed to understand and validate the experimental results, gaining insight into the widely used acoustic technique. © *2014 AIP Publishing LLC*. [http://dx.doi.org/10.1063/1.4897152]

Electrostatic potential barriers, i.e., double-Schottky barriers (DSBs), formed at the grain boundaries in various electroceramics such as ZnO, $BaTiO_3$, and $SrTiO_3$[1,2] are responsible for their unique properties, which are useful for commercial applications. However, the degradation of DSBs under electrical stress is hazardous to electroceramic devices and has become the focus of considerable interest.[3–5] The traditional techniques for characterizing the degradation of materials are centered around measuring the parameters of the materials,[4,6] rather than determining the inherent changes. Hence, many of the fundamental degradation mechanisms are poorly understood.

For ZnO-based electroceramics,[3] which is the vital protection component used as a surge arrester in energy transmission systems, the ion migration, which lowers the DSB,[7] is recognized as the cause of degradation, based on different circumstantial evidences[3] among the various aging theories that have been proposed. However, the motion and neutralization of charged ions in electroceramics have not been directly observed. Additionally, the identification of the main species of mobile ions among the numerous candidates is still uncertain and controversial.[6,8–10]

The lack of direct evidence of ion migration has made it difficult to clarify the physical processes that govern the electrical degradation of DSBs.[11] If insight into the degradation mechanism of DSBs can be gained, specific measurements could be adopted to effectively prolong the lifetimes of the devices. Recent successes in growing large-area and high-quality ZnO single crystals,[12,13] along with the established techniques in profiling the space charge distribution in dielectrics, have made it possible to trace the origin of the DSB degradation. In this paper, the pulsed electroacoustic (PEA) method[14] is performed on ZnO bicrystals[15] to observe the ion migration during the degradation process. This addresses the issue that has been pending for almost four decades on whether the degradation of the DSBs in electroceramics is caused by the migration and neutralization of defect ions. Furthermore, the results of the PEA measurements are validated with simulations by considering the attenuation effects of acoustic waves propagating in a lossy medium.

The nondestructive PEA method has been widely used over the past few decades to quantitatively detect the spatial distribution of charged ions in materials. This sensitive method with a high resolution[14] (R) around 0.13 nC/cm^2 and is a contemporarily effective technique, outweighing the other techniques that were developed for space charge distribution profiling, such as the Kerr electro-optic effect method ($R \approx 70$ nC/cm^2), the pressure wave pulse method ($R \approx 10$ nC/cm^2), and the pressure wave step method ($R \approx 20$ nC/cm^2).[16] The basic principle of the PEA method is as follows:[14] In accordance with Fig. 1, an applied electric pulse induced a perturbation force, causing the motion of charged ions inside the material. Then, the acoustic waves generated by this movement propagated in the through-thickness direction. Finally, a piezoelectric transducer, attached beneath the lower electrode, converted the waves into electrical signals, which were monitored by a high-speed oscilloscope. The amplitude of the signal was related to the charge density. The delay was related to the distance between the charges and the lower electrode. Hence, the output waveforms were straightforward and easy to comprehend. To determine the distribution of charged ions in ZnO electroceramics, a simplified structure was designed because performing measurements on conventional three-dimensional polycrystalline ceramic samples is beyond the detection limit[17] of the PEA method and can lead to incomprehensible output signals. The ZnO bicrystals,[15] in which a uniformly thin dopant layer was sandwiched between two ZnO single crystals of specific orientation, imitate an individual grain boundary in a electroceramic material. The distribution of charged ions in bicrystals is believed to only vary in the through-thickness direction.[14,17] Therefore, a bicrystal is a simplified structure that can be theoretically reduced to one-dimension and is appropriate for PEA tests.

Then, 20 mm (W) × 20 mm (L) × 2 mm (H) [0001] ZnO single crystals were grown using the hydrothermal method.[18] The contact surface was mechanochemically polished to a

[a]Author to whom correspondence should be addressed. Electronic mail: hejl@tsinghua.edu.cn. Fax: 86-01-62784709.

 © 2014 AIP Publishing LLC

This article is copyrighted as indicated in the article. Reuse of AIP content is subject to the terms at: http://scitation.aip.org/termsconditions. Downloaded to IP: 132.174.255.116 On: Tue, 23 Dec 2014 20:16:44

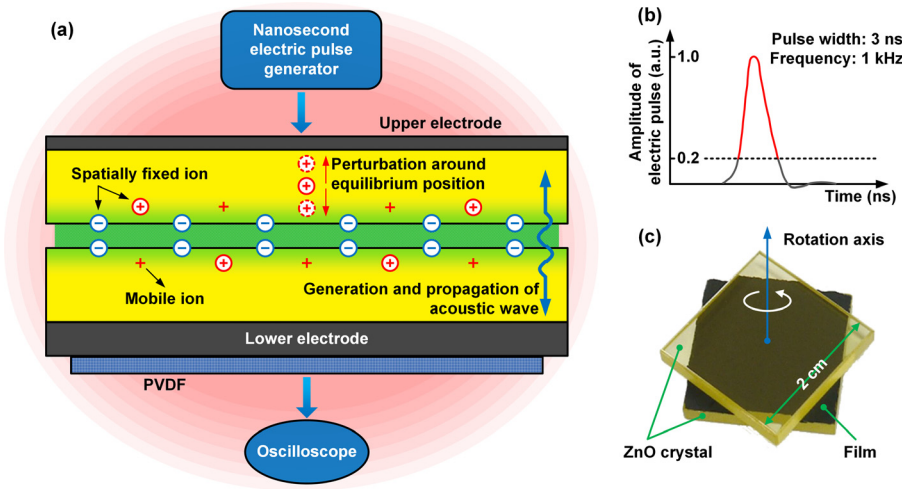

FIG. 1. (a) The basic principles of the PEA measurements on ZnO bicrystals. Under the perturbation of applied nanosecond electric pulses, the charged ions generate acoustic waves that propagate along the through-thickness direction of the bicrystal and are detected and converted into electric signals by an oscilloscope. PVDF stands for polyvinylidene fluoride. (b) The waveform of the applied nanosecond electric pulse. A pulse width of 3 ns was measured at the 20% rise time point. (c) A 20 mm (W) × 20 mm (L) × 2 mm (H) ZnO single crystal grown by a hydrothermal method. A thin dopant film (3 μm thick, obtained by tape casting, its composition shown in Table I) was inserted between two single crystals and the upper crystal was rotated coaxially to obtain the bicrystal structure, which was sintered at 1050 °C for 60 min and then cooled in a furnace.

mirror finish.[15] The dopant layer was a 3-μm-thick (dried) film, obtained by tape casting.[19] Its composition is outlined in Table I. All of the samples placed in the mold were sintered at 1050 °C for 60 min and then cooled in a furnace. ZnO [0001] bicrystals with a Σ7 coincidence site lattice twist boundary[15] were fabricated (see Fig. 1). A DSB was formed along the grain boundary in each bicrystal, confirmed by the nonlinear voltage-current characteristics in each sample.[15]

Bicrystal samples were continuously aged under a stabilized direct-current (DC) bias of +3 V at 320 K. After each 10-min period, positive electric pulses were applied to the samples to carry out the PEA measurements. Typical measurements of the ion distribution in the DSB region are shown in Fig. 2. Corresponding to Fig. S1 in the supplementary material,[20] the two positive parts of each curve (above 0 nC/cm^3) in Fig. 2 depict the distribution of the positively charged ions in the depletion layers. The negative part describes both the interfacial states and the inter-granular phases. Because the defect energy levels at the grain boundary interfaces are largely responsible for the electrical properties of ZnO electroceramics,[15] the inter-granular phases in the grain boundary were neglected in the following analysis. Figures 2(a) and 2(b) show that during the degradation process, the positive amplitude of the curve on the right side decreased continuously. However, the positive amplitude of the curve on the left side only decreased slightly. This indicated the lowering of the reverse-biased Schottky barrier. Moreover, along with the decrease in the number of negative ions, the geometric center of the negative part of the curve moved to the left, i.e., the magnitude of the right half of the negative curve was reduced significantly. Conversely, that of the left side remained almost unchanged. This can be interpreted as an asymmetrical reduction in the donor concentration in the two depletion layers. The above results indicate that the migration and neutralization of the charged ions mainly occurred in the reverse-biased Schottky barrier region in a bicrystal. When a voltage was applied, the reverse-biased Schottky barrier withstood most of the voltage. Compared with the positive ions in the forward-biased depletion layer, the ions in the reverse-biased region had a higher statistical probability of transiting and migrating to the grain boundary under the electrical stress. This is in accordance with Gupta's theoretical predictions with the instability model.[6] By comparing Figs. 2(a) and 2(b) for the reverse-biased barriers with different heights, their rates of aging are different. Using Poisson's equation,[3] it was calculated that the reverse-biased barrier of 0.68 eV (Fig. 2(a)) rapidly decreased by 26% within 120 min, while the barrier of 0.94 eV (Fig. 2(b)) dropped to 0.74 eV after an 800-min degradation test. This suggests that grain boundaries with higher reverse-biased barriers were more resistive to electrical degradation. It has been suggested that Zn_i^{2+} is the optimum candidate for the mobile ions.[6,9] To verify this, ZnO bicrystals underwent a brief aerobic oxidation (for 6 h) at 600 °C to eliminate the zinc interstitial defects[6,21] (related chemical reactions are detailed elsewhere[6]) and PEA measurements were performed. Even after a long-term degradation time of 50 h, the spatial ion distribution was almost invariant with time, as shown in Fig. 2(c).

To further understand and validate the measurements in Fig. 2, it was necessary to gain insight into the acoustic attenuation effects during the PEA measurements. Even though the research on attenuation recovery techniques[22] is favored for engineering applications, the mechanism of the

TABLE I. Composition of the aqueous tape casting slurry for the dopant films.

Material	Content (wt. %)	Function
Mixture of Bi_2O_3, MnO_2, and Co_2O_3	50.00	Dopant powder
Deionized water	41.40	Solvent
Polyvinyl alcohol	3.00	Binder
Ammonium polyacrylate	0.50	Dispersant
Glycerin	2.70	Plasticizer
Normal butanol	0.90	Defoamer
Span-20	1.50	Surfactant

This article is copyrighted as indicated in the article. Reuse of AIP content is subject to the terms at: http://scitation.aip.org/termsconditions. Downloaded to IP: 132.174.255.116 On: Tue, 23 Dec 2014 20:16:44

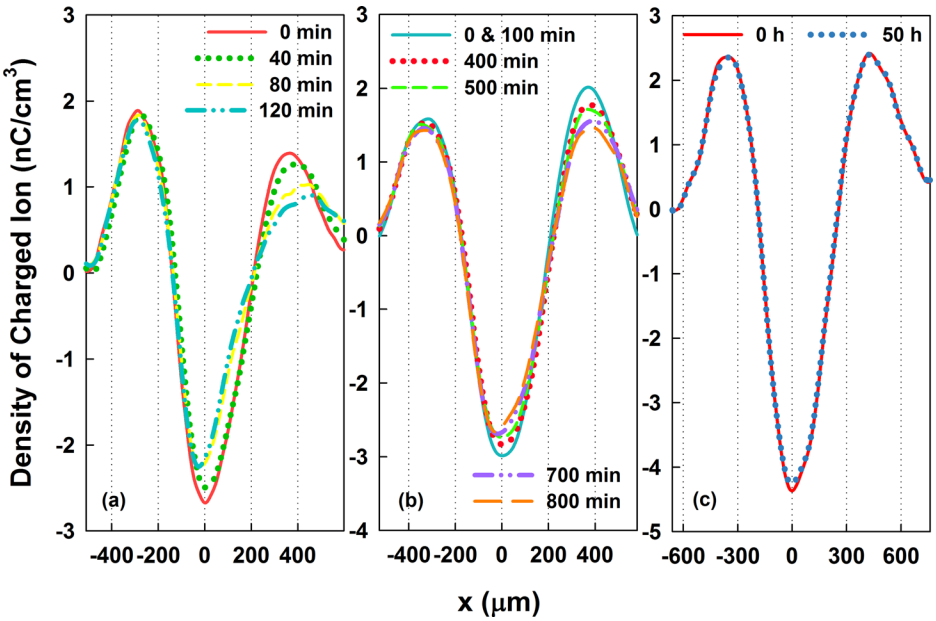

FIG. 2. Variation with time of the spatial distribution of charged ions in the DSB region during the degradation process. For each sample, the time indicated is the respective aging time under a stabilized DC bias of +3 V at 320 K. (a) and (b) are conventional bicrystal samples. (c) A bicrystal sample treated by aerobic oxidation. The grain boundary in a bicrystal is located at the zero-point on the horizontal axis.

acoustic attenuation involved in the PEA method, which is vital for interpreting complicated waveforms, is seldom discussed. Worse still, the literature is limited[16] and contains misleading information (inappropriate lossy wave equations). Therefore, the theoretical modeling of the propagation of waves in lossy mediums is described here. Because of the existence of liquid acoustic couplants, the longitudinal acoustic wave alone was considered, which was also required in the "one-dimension" assumption of the PEA method.[14,17] This process can be characterized by the propagation of the stress wave (denoted as $T(x,t)$).[16] In a lossy medium (such as a material sample or a wave guide), the stress plane wave propagates in the form[23]

$$T = cS + \eta \frac{\partial S}{\partial t}, \tag{1}$$

where $S(x,t)$ is the strain, c is the elastic constant of the material, t is the propagation time, and η is the viscosity coefficient of the medium. When a small time-variable stress is applied, the stress and strain in a material are related by the following two equations:[23,24]

$$\begin{cases} \rho_{m0} \dfrac{\partial^2 u}{\partial t^2} = \dfrac{\partial T}{\partial x} \\ S = \dfrac{\partial u}{\partial x}, \end{cases} \tag{2}$$

where $u(x,t)$ is the particle displacement in the material, x is the through-thickness direction and ρ_{m0} is the mass density in the stationary state. The above three equations were then combined to obtain the lossy wave equation

$$\frac{\partial^2 T}{\partial t^2} = \frac{c}{\rho_{m0}} \frac{\partial^2 T}{\partial x^2} + \frac{\eta}{\rho_{m0}} \frac{\partial}{\partial t} \left(\frac{\partial^2 T}{\partial x^2} \right) = V_a^2 \frac{\partial^2 T}{\partial x^2} + \alpha \frac{\partial^3 T}{\partial x^2 \partial t}, \tag{3}$$

where V_a is the acoustic wave velocity and α as the attenuation coefficient, used to correct and replace the inappropriate equation $\frac{\partial^2 T}{\partial x^2} = V_a^2 \frac{\partial^2 T}{\partial t^2} - \alpha \frac{\partial T}{\partial t}$, given in the literature.[16] Here, a brief discussion on the effect of the external electric field on the acoustic wave propagation is given for a small current situation (low conductivity), because the interactions between the drifting conduction electrons and acoustic waves may result in phenomena such as amplification[25,26] of the acoustic wave, which is beyond the scope of this paper and beyond the assumptions of the PEA method. When an electric field exists, an extra term should be added to the right side of Eq. (1) if the field causes additional stiffness.[24,27] And the effect of the electric field can be included in the variation of the elastic constant[24] such that the form of Eq. (3) can be kept constant. Moreover, during the PEA measurements, the viscosity played a dominant role, along with the electric field, in influencing the wave shape during propagation. To solve Eq. (3), the finite-difference time-domain method was employed and absorbing boundary conditions[28] were adopted in the simulations such that when an acoustic wave propagated across the boundary; it will be fully absorbed without reflecting.[29] For the DSB region discussed in this paper, the positively charged depletion layer was represented by a rectangular function, while the negative interfacial state was characterized by the Dirac function (Fig. 3) in the simulation

$$\delta(x - x') = \lim_{\beta \to 0} \left(\frac{1}{\beta \sqrt{\pi}} e^{-(x-x')^2/\beta^2} \right), \tag{4}$$

where β is the adjustable wave-shape coefficient.

The existence of acoustic-loss effects caused the width of the waveform to increase with time during propagation. For instance, an initially square wave becomes more and more Gaussian-like as it propagates away from its point of origin. Moreover, an exponential loss term proportional to the frequency squared was included in the theoretical model.[16] This indicates that the attenuation limits the propagation of the high-frequency components.[16] Thus, under the effect of acoustic attenuation, the two waves of the respective interfacial states became wider; gradually overlapping and eventually merging into a single negative waveform (see the "spread" and "final" curves in Fig. 3). The two waves in the respective depletion layers became much wider until they were captured by the polyvinylidene fluoride (PVDF)

This article is copyrighted as indicated in the article. Reuse of AIP content is subject to the terms at: http://scitation.aip.org/termsconditions. Downloaded to IP: 132.174.255.116 On: Tue, 23 Dec 2014 20:16:44

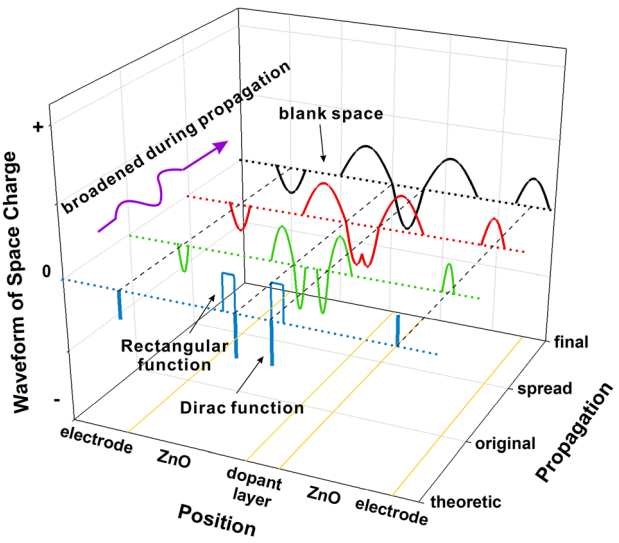

FIG. 3. The evolution of the waveforms, showing the distribution of the space charge. The "theoretic" curve is the ideal profile of the space charge in which a rectangular function was used for the donor density in the depletion layer for simplicity. For the interfacial states, a Dirac function was employed. The "original" curve represents the waveforms of the generated acoustic waves as soon as the nano-pulse was applied. The "spread" curve is the waveform during propagation, where the acoustic loss effects play a critical role in the widening of the wave. The "final" waveform is the signal recorded by the oscilloscope. In addition, the thickness of the dopant layer is deliberately enlarged to give a better resolution. This does not show the actual proportion of the inter-granular layer. (Multimedia view) [URL: http://dx.doi.org/10.1063/1.4897152.1]

sensor. This led to the results that are presented in Fig. 2. A similar effect took place on the interfacial sheet charge at the electrode. The final waveform of the sheet charge induced at the electrode surface was around 200 μm wide after it propagated through a ~4-mm-thick bicrystal and an aluminum waveguide that was several centimeters long. A long waveguide was needed to avoid acoustic reverberation. Thick ZnO single crystals are essential for separating the waveform of the sheet charge at the electrode surface and the waveforms of the DSB. This leaves blank spaces (see "final" curve in Fig. 3) between them, improving the resolution and validity because broadening caused by attenuation is inevitable. The output waveforms were broader than the theoretical predictions and contained adequate information on the DSB and were used to effectively characterize the variations in the DSB during its degradation. Moreover, based on the simulations described above, the waveforms in Fig. 2 can be easily calculated and approximated.[20]

In summary, the defect ion migration characteristics during the aging process in [0001] ZnO bicrystals under a DC bias were observed with PEA measurements. This study offers the possibility to experimentally access the predicted defect migration behavior and validates the aging theory proposed by Gupta and Carlson,[6] i.e., the degradation of a DSB is caused by ion migration, mainly at the reverse-biased Schottky barrier region inside the electroceramic. The mechanisms of the acoustic attenuation effects during the PEA measurements were described, broadening the understanding of the acoustic technique itself. Based on this, the propagation of waves in lossy mediums was simulated and the experimental results using PEA measurements on bicrystals were further validated.

We would like to extend sincere appreciation to Professor J. B. Bernstein (Ariel University) for the discussion on modeling the acoustic attenuation effects during the PEA measurements. We also acknowledge Professor Liuwan Zhang from the Department of Physics, Tsinghua University for his kind help in improving the overall quality of this paper. We would like to thank Pengfei Xu from the Department of Electrical Engineering, Tsinghua University for his advice on improving the numerical simulations by using the partial derivative equation and convey our sincere gratitude to Lei Han from the Ministry of Education Key Laboratory of Orogenic Belt and Crustal Evolution, School of Earth and Space Science, Peking University, for his support in the sample preparation and microstructure analysis. This paper benefitted from the use of the experimental facilities at the North China Electric Power University (NCEPU). We are grateful for the technical expertise on the PEA measurement provided by Professor Youping Tu (NCEPU). This work was supported by the National Nature Science Foundation of China under Grant No. 50737001 and by the 973 National Basic Research Program (Program No. 2014CB239504).

[1]Y. Sato, J. P. Buban, T. Mizoguchi, N. Shibata, M. Yodogawa, T. Yamamoto, and Y. Ikuhara, Phys. Rev. Lett. **97**, 106802 (2006).
[2]F. Greuter and G. Blatter, Semicond. Sci. Technol. **5**, 111 (1990).
[3]D. R. Clarke, J. Am. Ceram. Soc. **82**, 485 (1999).
[4]M. A. Ramirez, R. Tararam, A. Z. Simoes, A. Ries, E. Longo, and J. A. Varela, J. Am. Ceram. Soc. **96**, 1801 (2013).
[5]C. L. Cheng, J. Hu, and J. L. He, Mater. Lett. **132**, 240 (2014).
[6]T. K. Gupta and W. G. Carlson, J. Mater. Sci. **20**, 3487 (1985).
[7]G. E. Pike, Phys. Rev. B **30**, 795 (1984).
[8]R. Vidya, P. Ravindran, H. Fjellvag, B. G. Svensson, E. Monakhov, M. Ganchenkova, and R. M. Nieminen, Phys. Rev. B **83**, 045206 (2011).
[9]Y. S. Kim and C. H. Park, Phys. Rev. Lett. **102**, 086403 (2009).
[10]A. Janotti and C. G. Van de Walle, Phys. Rev. B **76**, 165202 (2007).
[11]D. C. Look, J. W. Hemsky, and J. R. Sizelove, Phys. Rev. Lett. **82**, 2552 (1999).
[12]F. Tuomisto, V. Ranki, K. Saarinen, and D. C. Look, Phys. Rev. Lett. **91**, 205502 (2003).
[13]Ü. Özgür, Ya. I. Alivov, C. Liu, A. Teke, M. A. Reshchikov, S. Doğan, V. Avrutin, S. J. Cho, and H. Morkoç, J. Appl. Phys. **98**, 041301 (2005).
[14]J. B. Bernstein, Phys. Rev. B **44**, 10804 (1991).
[15]C. L. Cheng, J. L. He, and J. Hu, Appl. Phys. Lett. **101**, 173508 (2012).
[16]J. B. Bernstein, Ph.D. thesis, Massachusetts Institute of Technology, 1990.
[17]Y. Li, M. Yasuda, and T. Takada, IEEE Trans. Dielectr. Electr. Insul. **1**, 188 (1994).
[18]E. Ohshima, H. Ogino, I. Niikura, K. Maeda, M. Sato, M. Ito, and T. Fukuda, J. Cryst. Growth **260**, 166 (2004).
[19]D. Hotza and P. Greil, Mater. Sci. Eng., A **202**, 206 (1995).
[20]See supplementary material at http://dx.doi.org/10.1063/1.4897152 for further information on prerequisite for PEA measurement, on theoretical analysis of acoustic attenuation effect during PEA measurement, on additional simulation results, and on reason for exclusion of directly bonded bicrystal.
[21]K. R. Kittilstved, D. A. Schwartz, A. C. Tuan, S. M. Heald, S. A. Chambers, and D. R. Gamelin, Phys. Rev. Lett. **97**, 037203 (2006).
[22]Y. Tanaka, K. Hanawa, K. Suzuki, and T. Takada, in *Proceedings of 2001 International Symposium on Electrical Insulating Materials* (2001), pp. 407–410.
[23]G. S. Kino, *Acoustic Waves: Devices, Imaging, and Analog Signal Processing* (Prentice-Hall, Englewood Cliffs, NJ, 1987), Vol. 107.
[24]A. R. Hutson and D. L. White, J. Appl. Phys. **33**, 40 (1962).
[25]H. N. Spector, Phys. Rev. **165**, 562 (1968).
[26]H. N. Spector, Phys. Rev. **127**, 1084 (1962).
[27]J. J. Kyame, J. Acoust. Soc. Am. **26**, 990 (1954).
[28]X. J. Yuan, D. Borup, J. Wiskin, M. Berggren, and S. A. Johnson, IEEE Trans. Ultrason., Ferroelectr., Freq. Control **46**, 14 (1999).
[29]J. C. Strikwerda, *Finite-Difference Schemes and Partial Differential Equations* (Wadsworth and Brooks, Pacific Grove, CA, 1989).

This article is copyrighted as indicated in the article. Reuse of AIP content is subject to the terms at: http://scitation.aip.org/termsconditions. Downloaded to IP: 132.174.255.116 On: Tue, 23 Dec 2014 20:16:44